http://dx.doi.org/10.5012/bkcs.2013.34.12.3635

CO Oxidation Activities of Ni and Pd-TiO_2@SiO_2 Core-Shell Nanostructures

Yeji Do, Insu Cho, Yohan Park, Debabrata Pradhan,† and Youngku Sohn*

*Department of Chemistry, Yeungnam University, Gyeongsan 712-749, Korea. *E-mail: youngkusohn@ynu.ac.kr*
†Material Science Centre, Indian Institute of Technology, Kharapur 721 302, W.B., India
Received July 31, 2013, Accepted September 12, 2013

We prepared Ni and Pd-modified TiO_2@SiO_2 core-shell nanostructures and then analyzed them by scanning electron microscopy, optical microscopy, X-ray diffraction crystallography, FT-IR and UV-Visible absorption spectroscopy. In addition, their CO oxidation performance was tested by temperature-programmed mass spectrometry. The CO oxidation activity showed an order of Ni-TiO_2@SiO_2 (900 °C) < Ni-TiO_2@SiO_2 (90 °C) < Ni-TiO_2@SiO_2 (450 °C) in the first CO oxidation run, and greatly improved activity in the same order in the second run. The $T_{10\%}$ (the temperature at 10% CO conversion) corresponds to the CO oxidation rate of 2.8×10^{-5} mol_{CO} g_{cat}^{-1} s^{-1}. For Ni-TiO_2@SiO_2 (450 °C), the $T_{10\%}$ was observed at 365 °C in the first run and at 335 °C in the second run. For the Pd-TiO_2@SiO_2 (450 °C), the $T_{10\%}$ was observed at a much lower temperature of 263 °C in the first CO oxidation run, and at 247 °C in the second run. The CO oxidation activities of transition metal modified TiO_2@SiO_2 core-shell nanostructures presented herein provide new insights that will be useful in developing catalysts for various environments.

Key Words : CO oxidation, TiO_2@SiO_2, Ni-TiO_2@SiO_2, Pd-TiO_2@SiO_2, Core-shell

Introduction

Removing toxic gases is very important for clean environments and respiratory biological systems.[1-3] Carbon monoxide (CO) is a toxic gas commonly produced from incomplete combustion of fossil fuels. Catalytic converters have played a major role in eliminating CO emission via the oxidation of CO to nontoxic CO_2 using a catalyst.[3] The CO oxidation reaction over transition metal oxide catalysts has been studied extensively in efforts to improve catalytic performance.[1] Among the many factors involved in oxidation performance, oxide supports and thermal pretreatments have been shown to be important key factors.[4-6] The use of silica (SiO_2) spheres as an oxide support in the development of catalysts has attracted a great deal of attention in recent years.[7-18] For example, Yan *et al.* prepared Co_3O_4 nanoparticles in SiO_2 nanocapsules and found a 100% CO conversion rate at 150 °C,[7] which was much better than that observed for other Co_3O_4 nanostructures such as nanowires with exposed reactive {111} planes. Ni@SiO_2, Co@SiO_2 and Fe@SiO_2 yolk-shell structures were prepared by Park *et al.* and shown to be good for steam reforming of methane with high temperature stability and recyclability.[11] Kim *et al.* coated SiO_2 with TiO_2 and ZrO_2 using a sol-gel method and embedded Pt. They found that Pt-support interaction became much stronger, and that CO oxidation performance was superior to that of uncoated Pt/SiO_2 and Pt/Al_2O_3.[8] Dye degradation under UV irradiation was tested for a transition metal catalyst with and without TiO_2/SiO_2 hybrid structures. The activity showed the order of Co-TiO_2/SiO_2 >> Co-TiO_2 > TiO_2/SiO_2 > Co-SiO_2 > TiO_2 > SiO_2,[12] reflecting the fact that the TiO_2/SiO_2 hybrid structure shows a higher synergic effect due to increased surface defects through the formation of Si-O-Ti bonds. $AuCuO_x$ hybrid nanocrystals were supported on silica, which resulted in the catalyst becoming more active and selective for acetaldehyde formation from ethanol.[5] SiO_2 has also been used to support Au and Ag nanoparticles.[13-18] In tests of the use of Ag/SiO_2 and Au/SiO_2 catalysts for CO oxidation, size and thermal pretreatment were shown to be important factors.

In the present study, we employed nonreducible SiO_2 as a base oxide support, and then coated the surface with reducible TiO_2. In this process, TiO_2 acts as a good interfacial binder for transition metals and surface oxygen defect sites. Additionally, Ni and Pd were used as transition metals for comparison and different annealing temperatures were applied before testing the CO oxidation activity. We chose the two different metals because they are positioned in the same group 10 of the periodic table, but have different outer electron configurations of [Ar] $4s^2$ $3d^8$ (or [Ar] $4s^1$ $3d^9$) and [Kr] 4d,[10] respectively. However, the oxidation state of 2+ for NiO and PdO show the same d^8 electron configuration.

Experimental

SiO_2 sphere oxide supports were synthesized by the Stöber method.[19] To coat the SiO_2 surface with TiO_2, we dispersed 1.0 g of SiO_2 powders in 50 mL ethanol, added 1.0 mL of titanium tetraisopropoxide, and then ultra-sonicated the mixed solution for 3 h, which yielded white TiO_2@SiO_2 catalysts. After the reaction, the powder products were first fully washed with ethanol only, then redispersed in 25.0 mL ethanol. Next, 10.0 mL of 0.1 M Ni(II) or 0.01 M Pd(II) solution was added to deposit Ni or Pd on the TiO_2@SiO_2 core-shell structures, after which the mixed solution was ultra-sonicated for 3 h. The final powder products were fully

washed with water and ethanol repeatedly. The powder samples were then dried at 90 °C in an oven, which yielded green and gray Ni-TiO_2@SiO_2 and Pd-TiO_2@SiO_2, respectively. The dried Ni-TiO_2@SiO_2 samples were subsequently annealed at 450 °C and 900 °C, while the Pd-TiO_2@SiO_2 sample was annealed at 450 °C. All samples were annealed in a conventional furnace. The surface morphologies and the colors of the as-prepared and annealed samples were examined by scanning electron microscopy (SEM, Hitachi S-4800) and optical microscopy, respectively. The X-ray diffraction (XRD) patterns were generated using a PANalytical X'Pert Pro MPD diffractometer with Cu Kα radiation (40 kV and 30 mA). UV-Vis absorption spectra for the powder samples were obtained using a Varian Cary 5000 UV-Vis-NIR spectrophotometer. FT-IR spectra were measured using a Thermo Scientific Nicolet iS10 spectrometer in attenuated total reflection mode. The CO oxidation performance was tested using a SRS RGA200 quadrupole mass spectrometer at a heating rate of 20 K/min under a mixture of CO (1%) and O_2 (2.5%) in N_2, with a flow rate of 40 mL/min. For the CO oxidation in a flow reactor, we used 10 mg of the sample in a quartz U-tube (with an inner diameter of 4 mm).

Results and Discussion

Figure 1 shows the SEM images of bare SiO_2, TiO_2-coated SiO_2 (TiO_2@SiO_2 core-shell), Ni and Pd-modified TiO_2@SiO_2 core-shells annealed at various temperatures. The SEM images of bare SiO_2 show a smooth surface and fairly uniform sphere shape with a diameter of about 200-300 nm. For the TiO_2-coated SiO_2, the surface became rougher and larger. The bare SiO_2 and TiO_2@SiO_2 were white. Upon modification with Ni (Ni-TiO_2@SiO_2, 90 °C-dried), the surface and the color of TiO_2@SiO_2 particles were dramatically changed, and the SiO_2 spheres became aggregated. The color of the sample was pale green. Upon annealing at 450 °C, the over-coated Ni complex decomposed to form islands on the TiO_2@SiO_2 surface. The islands became bigger upon annealing at a higher temperature of 900 °C. The colors of the 450 °C and 900 °C annealed samples (Ni-TiO_2@SiO_2,

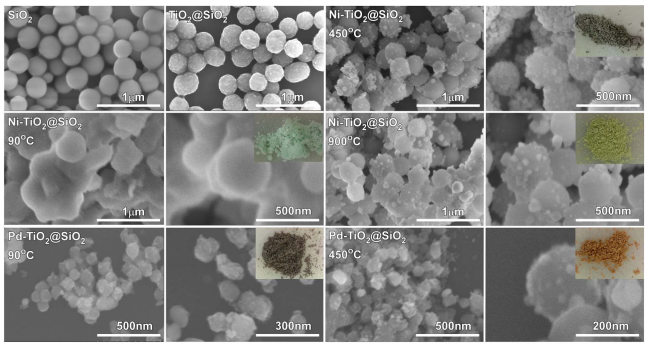

Figure 1. SEM images of bare SiO_2, TiO_2@SiO_2 core-shell, 90 °C-dried, 450 °C and 900 °C-preannealed Ni-TiO_2@SiO_2 core-shell catalysts, and 90 °C-dried, 450 °C-preannealed Pd-TiO_2@SiO_2 core-shell catalysts. The optical microscope images show the colors of the corresponding samples.

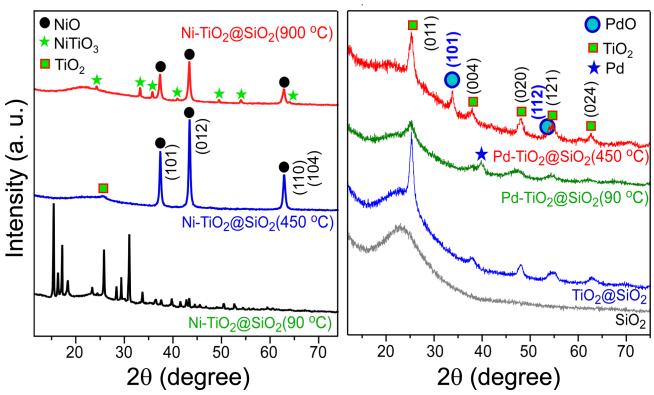

Figure 2. Powder X-ray diffraction patterns of bare SiO_2 spheres, TiO_2@SiO_2 core-shell structures, 90 °C-dried, 450 °C and 900 °C-preannealed Ni-TiO_2@SiO_2 catalysts, and 90 °C-dried and 450 °C-preannealed Pd-TiO_2@SiO_2 catalysts.

450 °C and 900 °C) showed gray-light green and yellow-green colors, respectively. Upon Pd modification (Pd-TiO_2@SiO_2, 90 °C-dried), the color changed to gray. Upon annealing at 450 °C (Pd-TiO_2@SiO_2, 450 ºC), the color changed to light-chocolate, and islands on the TiO_2@SiO_2 surface were observed.

Figure 2 displays the XRD patterns of bare SiO_2 sphere particles, TiO_2@SiO_2 core-shell structures, 90 °C-dried, 450 °C and 900 °C-preannealed Ni-TiO_2@SiO_2 catalysts, and 90 °C-dried and 450 °C-preannealed Pd-TiO_2@SiO_2 catalysts. For bare SiO_2, a very broad peak was found at around 22°, which is consistent with previous studies.[19] Upon coating with TiO_2 followed by annealing at 450 °C (TiO_2@SiO_2 core-shell structures), sharper peaks were found at 2θ = 25.3°, 37.9°, 48.2°, 54.6°, and 62.7°. These findings are in good agreement with those of the tetragonal anatase TiO_2 structure (JCPDS 1-084-1286), and were assigned to (011), (004), (020), (121) and (024) planes, respectively. Upon modifying the surface of TiO_2@SiO_2 catalysts with Ni and drying at 90 °C, various sharp XRD peaks were observed, possibly due to Ni complex formation on the surface. Upon annealing at 450 °C, three strong peaks appeared at 2θ = 37.3º, 43.3º, and 62.9º. These peaks were found to correspond to the (101), (012), and (110)/(104) planes of rhombohedral (R-3m) NiO (JCPDS 44-1159, a = b =2.96 Å, c = 7.23 Å).[20] Further annealing at 950 °C resulted in new XRD patterns in addition to those of NiO. The XRD peaks matched those of rhombohedral (R-3) $NiTiO_3$ (JCPDS 1-085-0451, a = b = 5.45 Å) well.[21] These findings indicate that nickel titanium oxide was formed at the interface between NiO and TiO_2@SiO_2. The XRD peak of TiO_2 was not observed due to the reaction between TiO_2 and thick Ni forming $NiTiO_3$.[22]

Figure 3 displays the UV-visible reflectance absorption spectra of bare SiO_2 sphere particles, 90 °C-dried, 450 ºC and 900 ºC-preannealed Ni-TiO_2@SiO_2 catalysts, and 90 ºC-dried and 450 ºC-preannealed Pd-TiO_2@SiO_2 catalysts. The optical microscope images (inset) show the colors of the corresponding samples. The Kubelka-Munk method was used to convert the diffuse reflectance to the absorbance (Y-

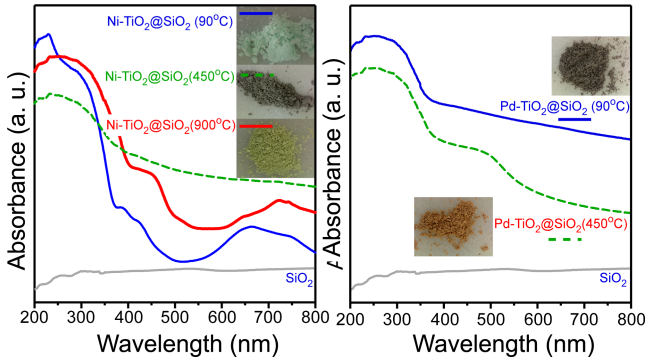

Figure 3. UV-Visible diffuse reflectance absorption spectra of bare SiO_2 spheres, 90 °C-dried, 450 °C and 900 °C-preannealed Ni-TiO_2@SiO_2 catalysts, and 90 °C-dried and 450 °C-preannealed Pd-TiO_2@SiO_2 catalysts.

axis). For bare white SiO_2, no discernible absorption peak was observed in the UV-Visible region. For the 90 ºC-dried Ni-TiO_2@SiO_2 catalyst, two broad absorption regions were found at around 250 nm and 650 nm. The broad band at around 650 nm was related to the absorption of Ni(II) ions. The band below 400 nm was likely due to a band gap absorption of the samples.[24] For the 450 ºC-preannealed Ni-TiO_2@SiO_2 sample, the absorption band of NiO was very broad, and covered the entire visible range.[24] As a result, the sample appeared gray. The UV-vis absorption spectrum of the 900 ºC-preannealed Ni-TiO_2@SiO_2 sample was similar to that of the 90 ºC-dried Ni-TiO_2@SiO_2 sample, but shifted to a longer wavelength. The band at 450 nm could be attributed to the Ni(II)Ti(IV) charge-transfer band arising from $NiTiO_3$.[25] The 90 ºC-dried Pd-TiO_2@SiO_2 catalyst was gray and its absorption covered the entire visible range. For the 450 ºC-annealed Pd-TiO_2@SiO_2 sample, the broad absorption at around 470 nm was attributed to PdO.[26]

Figure 4 shows the FT-IR spectra of bare SiO_2, TiO_2@SiO_2

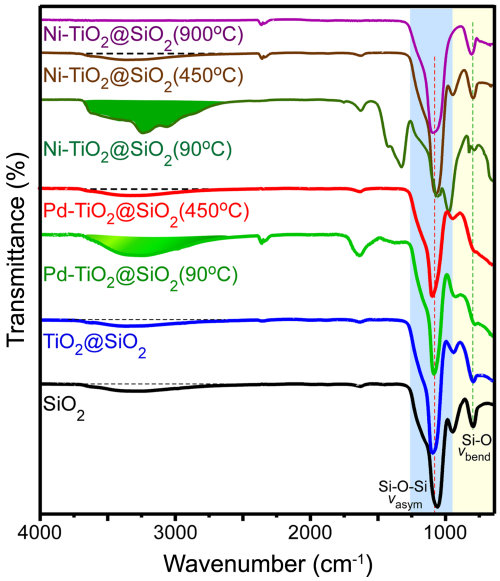

Figure 4. FT-IR spectra of bare SiO_2, TiO_2@SiO_2 core-shell, 90 ºC-dried, 450 ºC and 900 ºC-preannealed Ni-TiO_2@SiO_2 catalysts, and 90 ºC-dried, 450 ºC-preannealed Pd-TiO_2@SiO_2 catalysts.

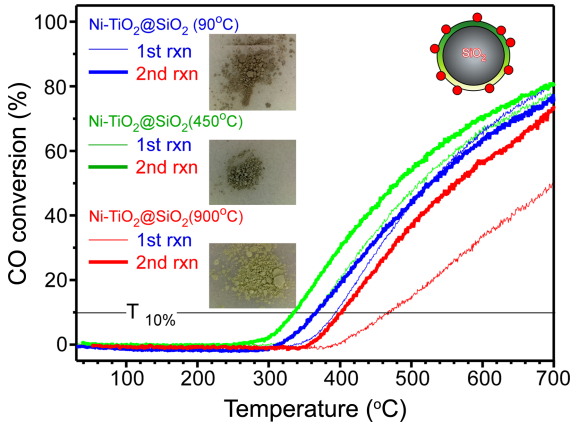

Figure 5. CO oxidation conversion (%) profiles for the first and second CO oxidation runs of 90 ºC-dried, 450 ºC and 900 ºC-preannealed Ni-TiO_2@SiO_2 catalysts. Inset optical microscope images show the color of the samples after the CO oxidation reaction.

core-shell, 90 ºC-dried, 450 ºC-preannealed, and 900 ºC-preannealed Ni-TiO_2@SiO_2 catalysts, and 90 ºC-dried, 450 ºC-preannealed Pd-TiO_2@SiO_2 catalysts. In the FT-IR spectra of bare SiO_2, two major peaks were observed at 1070 and 800 cm^{-1} in the region of 650-1700 cm^{-1}, which were attributed to Si–O–Si and Si-O bending modes, respectively.[27] The two peaks were dominant for all samples, indicating that the coating thickness is thin enough to detect the IR absorption signal from the core SiO_2. The weak broad peak at about 3200 cm^{-1} is attributed to adsorbed water and -OH. The broad peak at 3200 cm^{-1} was strong for 90 ºC-dried Ni-TiO_2@SiO_2 and Pd-TiO_2@SiO_2 samples. In addition, some extra peaks were observed due to vibrational modes of Pd or Ni complexes.[28] Upon annealing at 450 ºC, the broad peak intensity was dramatically diminished, as expected. Upon annealing of the Ni-TiO_2@SiO_2 sample at 900 ºC, no peak was observed at around 3000 cm^{-1} due to absence of water and OH groups.

We tested the CO oxidation performance of all of the aforementioned samples. Since the bare SiO_2 and TiO_2@SiO_2 samples showed no CO oxidation activity between room temperature and 700 ºC these samples are not discussed further. Figure 5 displays the CO oxidation conversion (%) profiles *versus* reaction temperature (°C) for the first and second CO oxidation runs of 90 ºC-dried, 450 ºC and 900 ºC-preannealed Ni-TiO_2@SiO_2 catalysts. The corresponding Arrhenius plots (ln rate *versus* 1/T) between the CO conversion of 10% and 15% are shown in Figure 6. The reaction rate (v) was calculated by the equation v = (molar CO flow rate, $mol \cdot s^{-1}$) × (CO conversion fraction)/(weight of the catalyst, g_{cat}). In the first run of 90 ºC-dried Ni-TiO_2@SiO_2 catalyst (Figure 5), the $T_{10\%}$ (the temperature at 10% CO_2 conversion) was observed at 395 °C, corresponding to an oxidation rate of 28 $mmol_{CO}\ s^{-1}\ g_{cat}^{-1}$. In the second run of CO oxidation, the $T_{10\%}$ decreased to 368 ºC, indicating that the activity was increased. For the 450 ºC-preannealed Ni-TiO_2@SiO_2 catalyst, the CO oxidation activity was greatly improved, and the $T_{10\%}$ was observed at 368 ºC

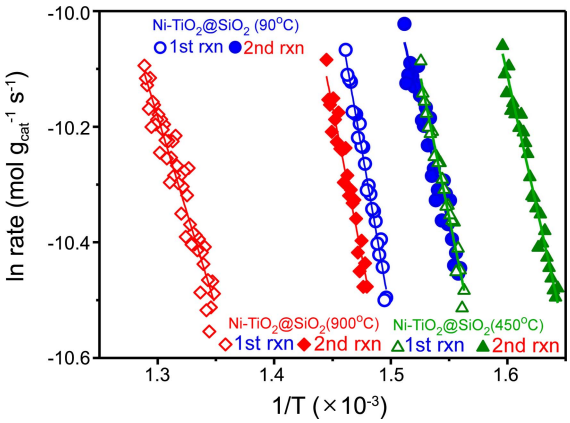

Figure 6. Arrhenius plots of the first and second CO oxidation runs of 90 ºC-dried, 450 ºC and 900 ºC-preannealed Ni-TiO_2@SiO_2 catalysts.

Table 1. Kinetic parameters for the 1st and 2nd second CO oxidation runs of 90 ºC-dried, 450 ºC-preannealed, and 900 ºC-preannealed Ni-TiO_2@SiO_2 catalysts

Catalysts	Oxidation rate[a] 1st/**2nd** at 400 ºC	E_a (kJ/mol)[b] 1st/**2nd**	$T_{10\%}$ (ºC) 1st/**2nd**
Ni-TiO_2@SiO_2 90 ºC	0.32/**0.51**	96.3/**68.9**	395/**368**
Ni-TiO_2@SiO_2 450 ºC	0.54/**0.85**	81.9/**75.7**	368/**335**
Ni-TiO_2@SiO_2 900 ºC	0.012/**0.26**	54.9/**85.4**	471/**402**

[a]The unit is $\times 10^{-4}$ mol_{CO} g_{cat}^{-1} s^{-1} for the CO oxidation rate. [b]The activation energy was measured in the CO conversion range of 10-15%.

and 335 ºC in the first and second runs of CO oxidation, respectively. However, for the Ni-TiO_2@SiO_2 catalysts pre-annealed at 900 ºC, the CO oxidation activity was degraded significantly, and the $T_{10\%}$ was observed at 471 ºC and 402 ºC in the first and second runs, respectively. Each sample showed different CO oxidation activities and colors after the reaction.

Table 1 summarizes the calculated kinetic parameters based on the CO conversion profiles (Figure 5) and the Arrhenius plots (Figure 6). In the first run, the CO oxidation rates at 400 °C were measured to be 0.32×10^{-4}, 0.54×10^{-4} and 0.012×10^{-4} mol g_{cat}^{-1} s^{-1} for the 90 ºC-dried, 450 ºC and 900 ºC-preannealed Ni-TiO_2@SiO_2 catalysts, respectively. The rates were increased to 0.51×10^{-4}, 0.85×10^{-4} and 0.26×10^{-4} mol g_{cat}^{-1} s^{-1} in the second run, respectively. The activation energies (E_a, kJ/mol) in the first run were measured to be 96.3, 81.9, and 54.9 kJ/mol, respectively, while these values were greatly reduced to 68.9, 75.7, and 85.4 kJ/mol, respectively, in the second run.

It is worth comparing our results with the CO oxidation rate and the thermal treatment effects of pure NiO samples. Wang *et al.* synthesized NiO nanorings and found CO oxidation rates of $0.38–2 \times 10^{-4}$ mol_{CO} g_{cat}^{-1} s^{-1}, which is in good agreement with our results.[6] They also observed that samples preannealed at 550 ºC showed the best performance,

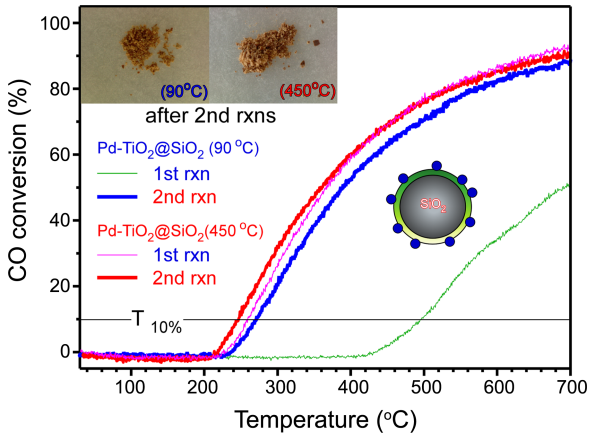

Figure 7. CO oxidation conversion (%) profiles for the first and second CO oxidation runs of 90 ºC-dried and 450 ºC-preannealed Pd-TiO_2@SiO_2 catalysts. Inset optical microscope images show the color of the samples after CO oxidation reaction.

and that catalytic activity was found to decrease above the annealing temperature. This observation is in good agreement with our temperature dependent result.

Figure 7 shows the CO oxidation conversion (%) profiles for the first and second runs of 90 ºC-dried and 450 ºC-preannealed Pd-TiO_2@SiO_2 catalysts. The corresponding Arrhenius plots (ln rate *versus* 1/T) are displayed in Figure 8. In the first run of 90 ºC-dried Pd-TiO_2@SiO_2 catalyst (Figure 7), the $T_{10\%}$ was observed at 495 °C. In the second run, the $T_{10\%}$ was significantly decreased (by 224 °C) to 271 °C. The significant decrease in temperature indicates that the catalyst became more active at a lower temperature. Based on the XRD and FT-IR data, Pd complex changes to PdO after high temperature thermal annealing, indicating that until the Pd complex changes to active PdO, CO oxidation may not occur. As a result, the onset CO oxidation temperature in the first run was much higher than in the second run. For the 450 ºC-preannealed Pd-TiO_2@SiO_2 catalyst, the CO oxidation activity was greatly improved, even in the first run. The $T_{10\%}$ was observed at 263 ºC and 247 ºC and in the first and second runs of CO oxidation, respectively.

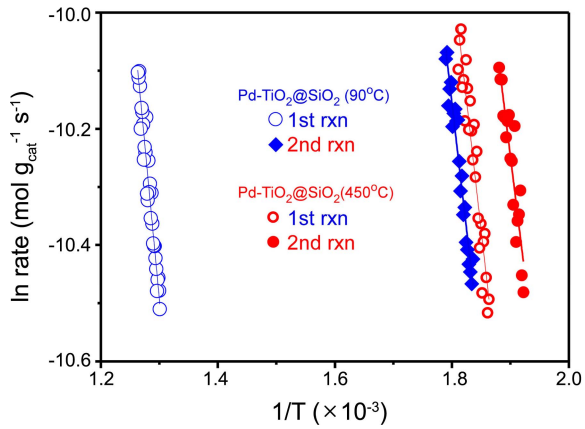

Figure 8. Arrhenius plots for the first and second CO oxidation runs of 90 ºC-dried, 450 ºC-preannealed Pd-TiO_2@SiO_2 catalysts.

Table 2. Kinetic parameters for the 1st and 2nd second CO oxidation runs of 90 ºC-dried and 450 ºC-preannealed Pd-TiO$_2$@SiO$_2$ catalysts

Catalysts	Oxidation rate[a] 1st/**2nd** at 400 ºC	E$_a$ (kJ/mol)[b] 1st/**2nd**	T$_{10\%}$ (ºC) 1st/**2nd**
Ni-TiO$_2$@SiO$_2$ 90 ºC	0.32/**0.51**	96.3/**68.9**	395/**368**
Ni-TiO$_2$@SiO$_2$ 450 ºC	0.54/**0.85**	81.9/**75.7**	368/**335**
Ni-TiO$_2$@SiO$_2$ 900 ºC	0.012/**0.26**	54.9/**85.4**	471/**402**

[a]The unit is $\times 10^{-4}$ mol$_{CO}$ g$_{cat}^{-1}$ s^{-1} for the CO oxidation rate. [b]The activation energy was measured in the CO conversion range of 10-15%.

The calculated kinetic parameters are summarized in Table 2 for the Pd-TiO$_2$@SiO$_2$ catalysts. In the first run, the CO oxidation rates at 500 °C were 0.30×10^{-4} and 2.0×10^{-4} mol g$_{cat}^{-1}$ s^{-1} for the 90 ºC-dried and 450 ºC-preannealed Pd-TiO$_2$@SiO$_2$ catalysts, respectively. For the 90 ºC-dried sample, the rate was dramatically increased to 1.95×10^{-4} mol g$_{cat}^{-1}$ s^{-1} in the second run, possibly due to formation of PdO with higher catalytic activity.[23] For the 450 ºC-preannealed sample, the rate was slightly increased in the second run when compared to the first run. Enhanced catalytic performance in the second run was also observed for other catalytic systems such as the metal-organic framework-supported Pd nanoparticles.[29] The activation energies (E$_a$) in the first run were measured to be 88.6 and 74.0 kJ/mol, respectively. In the second run, the values were measured to be 73.0 and 68.5 kJ/mol, respectively.

Based on the results for the two different catalyst systems, the Pd catalyst showed the much lower CO conversion temperature (or more energetically efficient catalytic performance) than the Ni catalyst. We further tested the stability[29] of the two selected catalysts (Ni-TiO$_2$@SiO$_2$ and Pd-TiO$_2$@SiO$_2$ 450 ºC). Figure 9 displays T$_{10\%}$ (°C) up to fourth runs, and CO conversion with reaction time at a fixed temperature (at 550 ºC for Ni-TiO$_2$@SiO$_2$, and at 450 ºC for Pd-TiO$_2$@SiO$_2$ 450 ºC catalysts). The T$_{10\%}$ was commonly

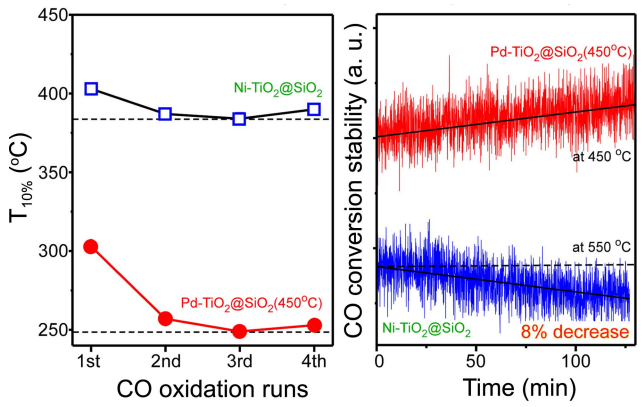

Figure 9. T$_{10\%}$ (left) for the 1st, 2nd, 3rd and 4th CO oxidation runs, and CO conversion with time at a selected temperature (right) for Ni-TiO$_2$@SiO$_2$ and Pd-TiO$_2$@SiO$_2$ 450 ºC catalysts.

decreased in the 2nd run, compared with the 1st run, as discussed above. The T$_{10\%}$ in the 3rd and 4th runs was not greatly different from that of the 2nd run within 10 ºC. The stability of the two catalysts was tested by measuring CO conversion with reaction time at a selected high temperature. In Figure 9 (right), the Pd-TiO$_2$@SiO$_2$ 450 ºC catalyst showed no decrease CO conversion while the Ni-TiO$_2$@SiO$_2$, catalyst shows 8% decrease in conversion yield after 2 h. This indicates that Pd-TiO$_2$@SiO$_2$ catalyst shows much better stability than Ni-TiO$_2$@SiO$_2$ catalyst.

Conclusion

We tested CO oxidation performance of Ni-TiO$_2$@SiO$_2$ and Pd-TiO$_2$@SiO$_2$ core-shell nanostructures and obtained CO conversion (%) profiles and Arrhenius plots *versus* reaction temperature. The CO oxidation rate (mol g$_{cat}^{-1}$ s^{-1}) occurred in the order of Ni-TiO$_2$@SiO$_2$ (900 ºC) < Ni-TiO$_2$@SiO$_2$ (90 ºC) < Ni-TiO$_2$@SiO$_2$ (450 ºC) in the first and second CO oxidation runs. For the Pd-TiO$_2$@SiO$_2$ catalysts, the oxidation rate occurred in the order of Pd-TiO$_2$@SiO$_2$ (90 ºC) < Pd-TiO$_2$@SiO$_2$ (450 ºC). The CO oxidation rate commonly increased in the second run when compared with the first run for the Ni-TiO$_2$@SiO$_2$ and Pd-TiO$_2$@SiO$_2$ core-shell catalysts. For the Ni-TiO$_2$@SiO$_2$ (450 ºC) catalyst, the T$_{10\%}$ (corresponding to a reaction rate of 2.8×10^{-5} mol$_{CO}$ g$_{cat}^{-1}$ s^{-1}) occurred at 368 ºC and 335 ºC in the first and second runs of CO oxidation with activation energies of 81.9 and 75.7 kJ/mol, respectively. For Pd-TiO$_2$@SiO$_2$ (450 ºC) catalyst, the T$_{10\%}$ occurred at much lower temperatures of 263 ºC and 247 ºC in the first and second runs with activation energies of 74.0 and 68.5 kJ/mol, respectively. The results of the present study confirm that the overlayer metal and thermal pretreatment are important factors for improving CO oxidation performance, and further highlight the importance of designing more efficient catalysts for environmental and chemical industrial applications.

Acknowledgments. This work was financially supported by the India-Korea joint project, the National Research Foundation of Korea (NRF) grant funded by the Korean government (MEST) (NRF-2011-0025386), and the Department of Science and Technology, New Delhi through the Indo-Korea/P-02 grant.

References

1. Royer, S.; Duprez, D. *ChemCatChem* **2011**, *3*, 24.
2. Xie, X.; Li, Y.; Liu, Z.-Q.; Haruta, M.; Shen, W. *Nature* **2009**, *458*, 746.
3. Twigg, M. V. *Appl. Catal. B* **2007**, *70*, 2.
4. Campbell, C. T.; Sharp, J. C.; Yao, Y. X.; Karp, E. M.; Silbaugh, T. L. *Faraday Discuss.* **2011**, *152*, 227.
5. Bauer, J. C.; Veith, G. M.; Allard, L. F.; Oyola, Y.; Overbury, S. H.; Sheng Dai, S. *ACS Catal.* **2012**, *2*, 2537.
6. Wang, D.; Xu, R.; Wang, X.; Li, Y. *Nanotechnol.* **2006**, *17*, 979.
7. Yan, N.; Chen, Q.; Wang, F.; Wang, Y.; Zhong, H.; Hu, L. *J. Mater. Chem. A* **2013**, *1*, 637.
8. Kim, M.-Y.; Choi, J.-S.; Toops, T. J.; Jeong, E.-S.; Han, S.-W.;

Schwartz, V.; Chen, J. *Catalysts* **2013**, *3*, 88.
9. Tian, C.; Chai, S.-H.; Mullins, D. R.; Zhu, X.; Binder, A.; Guo, Y.; Dai, S. *Chem. Commun*. **2013**, *49*, 3464.
10. Zeng, H. C. *Acc. Chem. Res*. **2013**, *46*, 226.
11. Park, J. C.; Bang, J. U.; Lee, J.; Ko, C. H.; Song, H. *J. Mater. Chem.* **2010**, *20*, 1239.
12. Zhao, N.; Yao, Y.; Feng, J.; Yao, M.; Li, F. *Water Air Soil Pollut*. **2012**, *223*, 5855.
13. Wang, R. H.; Wang, X. W.; John, H.; Xin, J. H. *ACS Appl. Mater. Interfaces* **2010**, *2*, 82.
14. Qian, K.; Luo, L.; Bao, H.; Hua, Q.; Jiang, Z.; Huang, W. *Catal. Sci. Technol*. **2013**, *3*, 679.
15. Zhang, X.; Qu, Z.; Li, X.; Wen, M.; Quan, X.; Ma, D.; Wu, J. *Sep. Purif. Technol*. **2010**, *72*, 395.
16. Yu, L.; Shi, Y.; Zhao, Z.; Yin, H.; Wei, Y.; Liu, J.; Kang, W.; Jiang, T.; Wang, A. *Catal. Commun.* **2011**, *22*, 616.
17. Tian, D.; Yong, G.; Dai, Y.; Yan, X.; Liu, S. *Catal. Lett*. **2009**, *130*, 211.
18. Afanasev, D. S.; Yakovina, O. A.; Kuznetsova, N. I.; Lisitsyn, A. S. *Catal. Commun*. **2012**, *22*, 43.
19. Wong, Y. J.; Zhu, L.; Teo, W. S.; Tan, Y. W.; Yang, Y.; Wang, C.; Chen, H. *J. Am. Chem. Soc*. **2011**, *133*, 11422.
20. Assaf, P. G. M.; Nogueira, F. G. E.; Assaf, E. M. *Catal. Today* **2013**, *213*, 2.
21. Urasaki, K.; Tanpo, Y.; Nagashima, Y.; Kikuchi, R.; Satokawa, S. *Appl. Catal. A* **2013**, *452*, 174.
22. Viktorov, V. V.; Belaya, E. A.; Serikov, A. S. *Inorg. Mater.* **2012**, *48*, 488.
23. Wang, S.-Y.; Li, N.; Zhou, R. M.; Jin, L.-Y.; Hu, G.-S.; Lu, J.-Q.; Luo, M.-F. *J. Mol. Catal. A* **2013**, *374*, 53.
24. Cui, Y.; Wang, C.; Wu, S.; Liu, G.; Zhang, F.; Wang, T. *CrystEngComm*. **2011**, *13*, 4930.
25. Qu, Y.; Zhou, W.; Ren, Z.; Du, S.; Meng, X.; Tian, G.; Pan, K.; Wang, G.; Fu, H. *J. Mater. Chem.* **2012**, *22*, 16471.
26. Zhang, Z.; Mestl, G.; Knozinger, H.; Sachtler, W. M. H. *Appl. Catal. A* **1992**, *89*, 155.
27. Jeon, H. J.; Yi, S.-C.; Oh, S.-G. *Biomater.* **2003**, *24*, 4921.
28. Nam, J. W.; Kim, K.-D.; Kim, D. W.; Seo, H. O.; Kim, Y. D.; Lim, D. C. *Curr. Appl. Phys*. **2012**, *12*, 429.
29. Kim, J. Y.; Jin, M.; Lee, K. J.; Cheon, J. Y.; Joo, S. H.; Kim, J. M.; Moon, H. R. *Nanoscale Res. Lett*. **2012**, *7*, 461.